Equivalent Circuit Models for Closed-loop Multiphysics Drive Systems

Pranav Chandran, Brian Johnson
Department of Electrical and Computer Engineering
University of Washington
Seattle, WA 98195
Email: {pchand2, brianbj}@uw.edu

Blake Rose
Department of Electrical and Computer Engineering
University of Wisconsin
Madison, WI 53706
Email: bdrose3@wisc.edu

***Abstract*—Power electronics drives are complex systems with coupled dynamical phenomena across electrical, control, and mechanical domains. This mix of heterogeneous subsystems obscures straightforward analysis, intuition, and design from an integrated system perspective. In this paper, we first show that each of these subsystems can be converted into an equivalent circuit. Leveraging the universality of energy, we stitch together a unified model where the closed-loop drive system is drawn as a single equivalent circuit. Focusing on permanent magnet synchronous machines with rotor saliency, drive control action is depicted as an RLC circuit, torques from d and q axis stator currents appear as current flows, electromechanical energy conversion is portrayed using an ideal transformer, inertia mimics capacitive storage, and the drivetrain also appears as a circuit. A simulation is provided where an end-to-end closed-loop electric vehicle system is modeled entirely as a circuit.**

I. Introduction

Equivalent circuit models have a rich history in both electrical [1] and mechanical engineering [2] disciplines. In both fields, such models have been instrumental in understanding how physical systems function. Despite that, equivalent circuit models within the electrical and mechanical communities have largely been pursued independently where use of mixed electromechanical models is scant. The main contribution of this paper lies in the key insight that such models can be interwoven into a unified equivalent circuit. The key insight that gives us unification is the universality of energy across all known physical domains. This paper builds on recent work [3], [4] where controllers are also cast as circuits, and ultimately we show how an end-to-end closed-loop drive system with speed and torque control can be modeled as a circuit.

Within the context of power electronics, equivalent circuit models were first formulated for open-loop converter modeling [5], [6]. Eventually, *impedance-based modeling* was introduced [7], [8] to include the effect of control feedback. Under such a framework, the output port of a converter is represented as a Norton or Thévenin equivalent and its impedances can be used to characterize stability. One limitation of this approach is that it gives a coarse two-element lumped circuit equivalent where many aspects of the control loop(s) and converter are either neglected, approximated, or obscured. Most recently, converters and their controls have been analyzed through the lens of circuit theory [3], [4]. By uncovering instances of Kirchhoff's laws within control loops, meshed multi-element circuit models follow along with accompanying analytical methods that link classical circuit and control theory.

Shifting focus to electromechanical systems, equivalent circuits for machine electrical dynamics form some of the earliest models used by the power community [9], [10]. In this setting, the back electromotive force (EMF), rotor, and stator are cast as a circuit model. On the other end, circuit equivalents for mechanical systems have a rich history where even James Clerk Maxwell uncovered connections [2], [11]. In such a setting, Newton's equations are analogous to Kirchhoff's Laws and allow for the derivation of circuits that exhibit dynamics identical to the original system [12]. Reflecting on this overview, it is clear that circuit equivalents have been widely used within the electrical and mechanical engineering communities. Aside from a few exceptions described below, electromechanical systems are typically represented as distinct electrical and mechanical subsystems despite being coupled. In [13], electromechanical transducers are modeled as equivalent circuits with transformers or gyrators linking physical domains. The synchronous generator and dc machine models in [14] and [15], respectively, outline coupled electrical-mechanical circuit models via ideal transformers or coupled dependent sources. Most relevant to the topic of drives, the works in [16], [17] establish a circuit representation that links electrical and mechanical dynamics by use of an ideal gyrator between physical domains.

In this paper, we leverage conservation of energy to establish a unified circuit framework that links control, electrical, and mechanical domains. Unlike in [16], [17], electromechanical conversion is captured via an ideal transformer as opposed to a gyrator, and control loops are also interwoven into our model. We also model machine saliency, which underpins flux-weakening methods, and illustrate the reluctance torque contribution in circuit format. A multiphysics circuit model, which encompasses speed and torque controls, machine dynamics, electromechanical energy conversion, and mechanical dynamics, is illustrated in an electric vehicle (EV) case study. Section II outlines the overall system structure. Circuit equivalents for each domain are established in Section III. The unified multiphysics model is derived in Section IV and simulations are in Section V. Concluding statements are in Section VI.

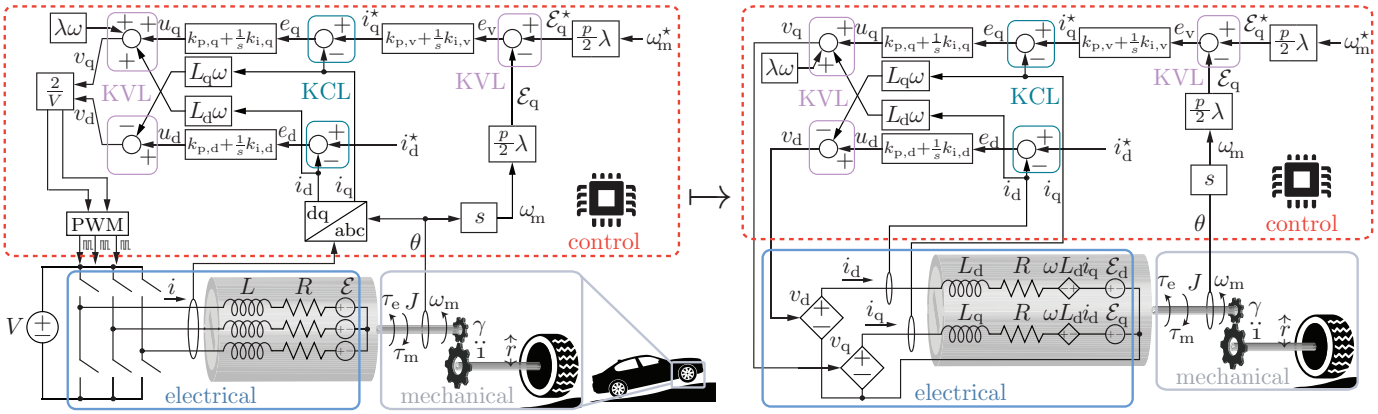

(a) switch-level drive system model (b) averaged synchronous frame model

Fig. 1: A switched model of a drive system is shown in (a) and its averaged counterpart in the synchronously rotating reference frame is given in (b). In both of these typical representations, the electrical, mechanical, and control subsystems are segregated from one another.

II. System Fundamentals and Notation

Consider the system in Fig. 1 which contains a three-phase power electronics drive, a permanent magnet synchronous machine with mechanical load, as well as inner and outer control loops which regulate torque and speed, respectively.

Electrical: The position of the rotor magnet north pole relative to the fixed a-phase coil is $\theta_{\rm m}$. From here forward, the power-invariant form of Park's transformation below is used.

$$\Gamma(\theta) := \sqrt{\frac{2}{3}} \begin{bmatrix} \cos\theta & \cos(\theta - \frac{2\pi}{3}) & \cos(\theta + \frac{2\pi}{3}) \\ -\sin\theta & -\sin(\theta - \frac{2\pi}{3}) & -\sin(\theta + \frac{2\pi}{3}) \end{bmatrix}. \quad (1)$$

In (1), θ is the electrical angle which can be expressed in terms of the pole count, p, and mechanical angle, $\theta_{\rm m}$, such that $\theta = p\theta_{\rm m}/2$. Electrical and mechanical speeds are defined as $\omega = d\theta/dt$ and $\omega_{\rm m} = d\theta_{\rm m}/dt$, respectively. Since the transformation in (1) acts on the electrical angle, all dq-based models hereafter are in the synchronous reference frame.

Three-phase stator currents, motion-induced back EMFs, and drive terminal voltages are denoted as $i = [i_{\rm a}, i_{\rm b}, i_{\rm c}]^\top$, $\mathcal{E}(\theta) = [\mathcal{E}_{\rm a}(\theta), \mathcal{E}_{\rm b}(\theta), \mathcal{E}_{\rm c}(\theta)]^\top$, and $v = [v_{\rm a}, v_{\rm b}, v_{\rm c}]^\top$, respectively. Assume a symmetric structure with identical stator coils with resistance R. Kirchhoff's Law gives $v = R_{\rm s} i + d(L_{\rm s}(\theta)i)/dt - \mathcal{E}(\theta)$ where $R_{\rm s} = I_3 R \in \mathbb{R}^{3\times 3}$ and I_3 is the 3×3 identity matrix. Faraday's Law gives $\mathcal{E}(\theta) = -d(\lambda_{\rm sr}(\theta))/dt$ where $\lambda_{\rm sr}(\theta) = N\phi[\cos\theta, \cos(\theta - 2\pi/3), \cos(\theta + 2\pi/3)]^\top$ is the rotor-to-stator flux linkage, N is the stator turn count, and ϕ is the peak magnet flux. The stator inductance matrix is

$$\begin{aligned} L_{\rm s}(\theta) &= LI_3 - \frac{L_{\rm m}}{2}(\mathbb{1}_3 - I_3) \\ &+ L_\theta \begin{bmatrix} \cos(2\theta) & 0 & 0 \\ 0 & \cos\left(2\theta - \frac{4\pi}{3}\right) & 0 \\ 0 & 0 & \cos\left(2\theta - \frac{2\pi}{3}\right) \end{bmatrix} \\ &+ \frac{L_{{\rm m}\theta}}{2} \begin{bmatrix} 0 & \cos\left(2\theta - \frac{2\pi}{3}\right) & \cos\left(2\theta - \frac{4\pi}{3}\right) \\ \cos\left(2\theta - \frac{2\pi}{3}\right) & 0 & \cos(2\theta) \\ \cos\left(2\theta - \frac{4\pi}{3}\right) & \cos(2\theta) & 0 \end{bmatrix}, \end{aligned} \quad (2)$$

where $\mathbb{1}_3 \in \mathbb{R}^{3\times 3}$ is a matrix with each entry equal to 1, $L_{\rm m}$ is the mutual inductance between any two stator coils, L_θ is the rotor angle dependence magnitude among the self inductances, and $L_{{\rm m}\theta}$ captures mutual inductance position dependence. The L_θ and $L_{{\rm m}\theta}$ terms in (2) represent machine *saliency*.

Establish the following in the synchronous frame: $v_{\rm dq} = [v_{\rm d}, v_{\rm q}]^\top = \Gamma(\theta)v$, $i_{\rm dq} = [i_{\rm d}, i_{\rm q}]^\top = \Gamma(\theta)i$, $\mathcal{E}_{\rm dq} = [\mathcal{E}_{\rm d}, \mathcal{E}_{\rm q}]^\top = \Gamma(\theta)\mathcal{E}(\theta)$, and $\lambda_{\rm dq} = [\lambda_{\rm d}, \lambda_{\rm q}]^\top = \Gamma(\theta)\lambda_{\rm sr}(\theta)$. Since $i = \Gamma^\top(\theta) i_{\rm dq}$, $\mathcal{E}(\theta) = \Gamma^\top(\theta)\mathcal{E}_{\rm dq}$, and $\Gamma(\theta)\Gamma^\top(\theta) = I_2 \in \mathbb{R}^{2\times 2}$, Kirchhoff's Law becomes

$$\begin{aligned} \begin{bmatrix} v_{\rm d} \\ v_{\rm q} \end{bmatrix} &= \Gamma(\theta)\big[R_{\rm s}\Gamma^\top(\theta) i_{\rm dq} \\ &\quad + \frac{d}{dt}(L_{\rm s}(\theta)\Gamma^\top(\theta) i_{\rm dq}) + \Gamma^\top(\theta)\mathcal{E}_{\rm dq}\big], \\ &= \begin{bmatrix} Ri_{\rm d} + L_{\rm d}\frac{di_{\rm d}}{dt} - \omega L_{\rm q} i_{\rm q} \\ Ri_{\rm q} + L_{\rm q}\frac{di_{\rm q}}{dt} + \omega L_{\rm d} i_{\rm d} + \mathcal{E}_{\rm q} \end{bmatrix}, \end{aligned} \quad (3)$$

where the second expression follows after well-known manipulations [9]. Above, $\mathcal{E}_{\rm q} = \omega\lambda$ where $\lambda = \sqrt{3/2}N\phi$ is the magnet flux linking the stator in the dq frame. Also,

$$\begin{aligned} L_{\rm d} &= \frac{L_{\rm m}}{2} + L + \frac{L_\theta + L_{{\rm m}\theta}}{2}, \\ L_{\rm q} &= \frac{L_{\rm m}}{2} + L - \frac{L_\theta + L_{{\rm m}\theta}}{2}. \end{aligned} \quad (4)$$

Control: A typical field-oriented speed controller is shown in Fig. 1 where all control signals are in the synchronous frame. Since $\mathcal{E}_{\rm q}$ is linearly proportional to angular velocity, speed control is achieved by manipulation of q axis signals. A mechanical speed command, $\omega^\star_{\rm m}$, is translated to the corresponding back EMF voltage command $\mathcal{E}^\star_{\rm q} = (p\lambda/2)\omega_{\rm m}$. The EMF voltage error, $e_{\rm v}$, is processed by a proportional-integral (PI) controller with proportional and integral gains $k_{\rm p,v}$ and $k_{\rm i,v}$, respectively. This outer speed controller yields the current command $i^\star_{\rm q}$ which is proportional to torque. For the sake of generality, assume $i^\star_{\rm d}$ is an arbitrary unspecified signal[1]. Current errors, denoted as $[e_{\rm d}, e_{\rm q}]^\top$, are processed by inner PI controllers with proportional and integral gains $[k_{\rm p,d}, k_{\rm p,q}]^\top$ and $[k_{\rm i,d}, k_{\rm i,q}]^\top$, respectively, and whose control

[1] $i^\star_{\rm d}$ is typically fixed at zero except in cases where flux-weakening is used.

effort is $[u_{\rm d}, u_{\rm q}]^\top$. After feedforward signals are added to the control effort, the inner torque controller yields the switch-cycle-averaged drive terminal voltages $[v_{\rm d}, v_{\rm q}]^\top$ which are in turn processed by a pulse width modulator. Averaging over one switch cycle and projecting all variables to the synchronous frame, we obtain the model in Figure 1(b).

Mechanics: The motor, shaft, gear, and wheel system have a combined angular inertia J, and the shaft experiences electrical and mechanical torques $\tau_{\rm e}$ and $\tau_{\rm m}$, respectively. Angular kinetic friction at the rotor shaft is denoted as $\beta_{\rm r}$ and frictional torque is $\beta_{\rm r}\omega_{\rm m}$. Terrain-to-wheel mechanical torque is transferred to the motor shaft across a gear with machine-side to drivetrain-side ratio γ:1.

The overall vehicle, payload, and passengers have total mass m. A wheel with radius r rolls on terrain with grade $\theta_{\rm g}$. This yields a tangential force on the wheel edge given by $F_{\rm g}(\theta_{\rm g}) = mg\sin\theta_{\rm g}$ where g denotes gravitational acceleration. We model rolling friction on the tires as the summation of speed-dependent and speed-independent forces given by $F_{\rm f}(\theta_{\rm g}) := mgf_0\cos\theta_{\rm g}$ and $v_{\rm m}\alpha(\theta_{\rm g})$, respectively, where f_0 and $f_{\rm v}$ are frictional coefficients, $v_{\rm m}$ is the vehicle velocity, and $\alpha(\theta_{\rm g}) := mgf_{\rm v}\cos\theta_{\rm g}$ resembles a grade-dependent damping. Assuming system rigidity, the vehicle translational velocity, mechanical angular velocity, and electrical angular velocity are related by

$$v_{\rm m} = \omega_{\rm m}\frac{r}{\gamma} = \omega\frac{2r}{p\gamma}. \tag{5}$$

Ignoring wind, the drag is

$$F_{\rm d}(v_{\rm m}) = \frac{1}{2}\rho C_{\rm d}{\rm A_f}v_{\rm m}^2, \tag{6}$$

where ρ is the density of air, C_d is the drag coefficient, $A_{\rm f}$ is the frontal area. These modeling constructs are in [18].

Rotational dynamics abide by

$$J\frac{d\omega_{\rm m}}{dt} = \tau_{\rm e} - \beta_{\rm r}\omega_m - \tau_{\rm gb}, \tag{7}$$

where $\tau_{\rm m} = \beta_{\rm r}\omega_m + \tau_{\rm gb}$ is the total mechanical torque and $\tau_{\rm gb}$ denotes the torque on the motor-side of the gearbox. Assuming an ideal gearbox and lossless energy transfer between angular and translational domains, the force delivered by the drivetrain, denoted as $F_{\rm t}$, to the wheel edge is $\tau_{\rm gb}\gamma/r$. This gives the following translational dynamics

$${\rm m}\frac{dv_{\rm m}}{dt} = F_{\rm t} - v_{\rm m}\alpha_{\rm t}(\theta_{\rm g}) - F_{\rm g}(\theta_{\rm g}) - F_{\rm f}(\theta_{\rm g}) - F_{\rm d}(v_{\rm m}). \tag{8}$$

III. Modeling Subsystems as Circuits

Before we obtain a unified circuit equivalent, we first uncover circuit representations for the stator, drive controls, and mechanical systems. Subsequently, conservation of energy is used to weave all subsystems into a single circuit.

A. Stator Dynamics as a Circuit

Here, we seek a streamlined circuit representation of the electrical machine dynamics in (3). Add and subtract $\omega L_{\rm d} i_{\rm d}$ from the first row of (3) to obtain

$$\begin{aligned}\begin{bmatrix} v_{\rm d} \\ v_{\rm q}\end{bmatrix} &= \begin{bmatrix} Ri_{\rm d} + L_{\rm d}\frac{di_{\rm d}}{dt} - \omega L_{\rm d} i_{\rm q} + \omega(L_{\rm d} - L_{\rm q})i_{\rm q} \\ Ri_{\rm q} + L_{\rm q}\frac{di_{\rm q}}{dt} + \omega L_{\rm d} i_{\rm d} + \omega\lambda\end{bmatrix}, \\ &= \begin{bmatrix} Ri_{\rm d} + L_{\rm d}\frac{di_{\rm d}}{dt} - \omega L_{\rm d} i_{\rm q} + \mathcal{E}_{\rm d} \\ Ri_{\rm q} + L_{\rm q}\frac{di_{\rm q}}{dt} + \omega L_{\rm d} i_{\rm d} + \mathcal{E}_{\rm q}\end{bmatrix},\end{aligned} \tag{9}$$

where $\mathcal{E}_{\rm d} := \omega(L_{\rm d} - L_{\rm q})i_{\rm q}$. The results of the d-axis manipulations in (9), and depicted in Fig. 1(b), are particularly appealing since, i) the net power absorbed by the d and q axis cross-coupling terms is zero (i.e., $(-\omega L_{\rm d} i_{\rm q})i_{\rm d} + (\omega L_{\rm d} i_{\rm d})i_{\rm q} = 0$), and ii) the power absorbed into the back EMF, namely $\mathcal{E}_{\rm d} i_{\rm d}$, is converted into mechanical torque. Observation (i) can be captured as a lossless two-port circuit element where the effective resistance of each input port is $\omega L_{\rm d}$. This is known as the *gyration* effect [19] and is represented by the ideal gyrator in Fig. 2 which transfers energy between axes. We close by noting that observation (ii) allows us to express the electrically-induced mechanical power as

$$\begin{aligned}\mathcal{E}_{\rm q} i_{\rm q} + \mathcal{E}_{\rm d} i_{\rm d} &= \underbrace{\lambda\frac{p}{2}\omega_{\rm m}}_{\mathcal{E}_{\rm q}} i_{\rm q} + \underbrace{\frac{p}{2}\omega_{\rm m}(L_{\rm d} - L_{\rm q})i_{\rm q}}_{\mathcal{E}_{\rm d}} i_{\rm d} \\ &= \tau_{\rm q}\omega_{\rm m} + \tau_{\rm d}\omega_{\rm m}, \\ &= \tau_{\rm e}\omega_{\rm m},\end{aligned} \tag{10}$$

where $\tau_{\rm e} = \tau_{\rm q} + \tau_{\rm d}$, and

$$\tau_{\rm q} = i_{\rm q}\left(\lambda\frac{p}{2}\right), \quad \tau_{\rm d} = i_{\rm d}\left(\frac{p}{2}(L_{\rm d} - L_{\rm q})i_{\rm q}\right). \tag{11}$$

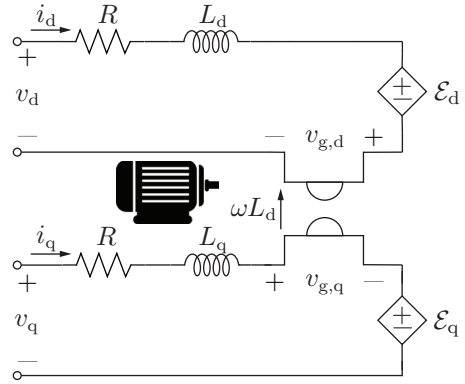

Fig. 2: Equivalent circuit of the machine stator dynamics where a gyrator captures cross-coupling between axes and EMFs are coupled with motion.

B. Controllers as Circuits

Torque Control: Referring to (11), we first note that torques are regulated via currents since they are proportional. Figure 1 reveals that the dq current compensators have current differences at their inputs and voltage signals on their output sides. This indicates an impedance-like behavior where we denote the d and q compensator transfer functions as the impedances $z_{\rm c,d}(s) := k_{\rm p,d} + k_{\rm i,d}/s$ and $z_{\rm c,q}(s) := k_{\rm p,q} + k_{\rm i,q}/s$, respectively. Uncovering Kirchhoff's relations in Fig. 1(b), the controller can be redrawn equivalently as in Figure 3. Evidently, the reference signals act as current sources, proportional and integral gains are identical to equivalent resistances

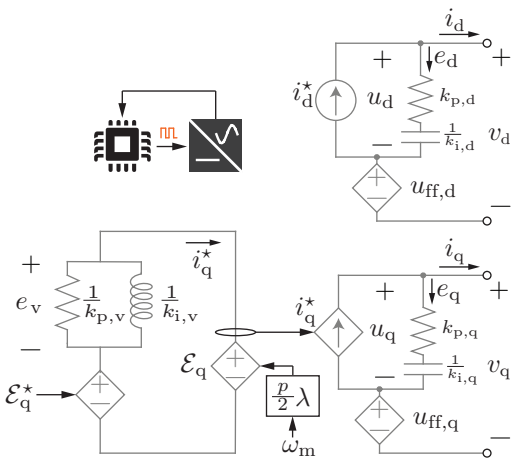

Fig. 3: Equivalent circuit of speed and torque controllers.

and inverse capacitances, the compensator itself is a series-connected RC circuit, and feedforward takes the form of a measurement-dependent voltage source.

Speed Control: Since $\mathcal{E}_\mathrm{q} = \lambda\omega_\mathrm{m}p/2$, speed regulation is tantamount to back EMF voltage regulation. Hereafter, we consider speed dynamics in terms of a back EMF voltage to emphasize the circuit nature of the model. Having said that, identical results could be obtained from mechanical relations directly. Given that the speed controller in Fig. 1 converts voltage differences into a current command, the compensator mimics an admittance given by $z_\mathrm{c,v}^{-1}(s) := k_\mathrm{p,v} + k_\mathrm{i,v}/s$. As shown in Fig. 3, the parameters $k_\mathrm{p,v}$ and $k_\mathrm{i,v}$ are mapped to a conductance and inverse inductance, respectively, where the EMF error is placed across a parallel RL branch and the speed command is a voltage source. Evidently, the speed and torque control loops exhibit dual structures as highlighted in [3], [4].

C. Vehicle Mechanics as a Circuit

The crux of the mechanical-to-circuit equivalent lies in drawing parallels between a system's equations of motion and electrical laws, while also defining appropriate force (voltage) and flow (current) variables. Multiple analogies are possible, the choice of which results in either transformers or gyrators linking physical domains [16]. Here, we select torque and force as current-like quantities, angular speed and velocity as proxies for voltage, and the moment of inertia and mass as capacitances. Since (torque $\times$ speed) and (force $\times$ velocity) are equal to power, this ties our model to energy.

Compare the Newtonian equations in (7)–(8) and a capacitor state equation of the form $\widetilde{C}d\widetilde{v}/dt = \widetilde{i}_\mathrm{c}$. Hence, (7) and (8) can each be depicted as a circuit where the moment of inertia, J, and mass, m, become equivalent capacitances. Furthermore, the right-hand-sides of (7)–(8) mirror Kirchhoff's Current Law. It follows that the rotational shaft friction β_r maps to a conductance across the equivalent capacitance J and the translational damping $\alpha_\mathrm{t}(\theta_\mathrm{g})$ acts as a parallel-connected conductance across equivalent capacitance m. In (7), the drive torque, τ_e, is represented as a current injected into capacitance J. Forces associated with gravity and speed-independent friction, $F_\mathrm{g}(\theta_\mathrm{g})$ and $F_\mathrm{f}(\theta_\mathrm{g})$, respectively, in (8) act as current sinks and the drag force, $F_\mathrm{d}(v_\mathrm{m})$, becomes a nonlinear state-dependent current. To link the rotational and translational domains into a single circuit, we note that lossless power transfer across the gearbox and wheel structure give

$$\omega_\mathrm{m}\tau_\mathrm{gb} = F_\mathrm{t}v_\mathrm{m}. \tag{12}$$

Rigidity between rotational and mechanical domains and energy conservation in (12) map to equivalent transformer action. The observations above collectively give Figure 4.

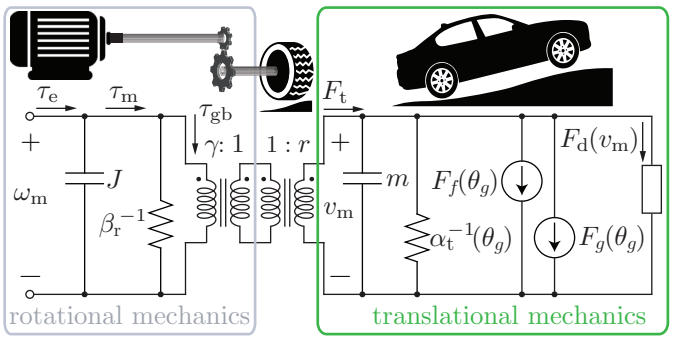

Fig. 4: The mechanical system of an electric vehicle represented as an equivalent circuit.

IV. Unified Multiphysics Model

Our main result of a unified circuit model will now be obtained by application of energy conservation and Kirchhoff's Laws. Once the unified model is in hand, we then show that closed-loop dynamics with control are straightforwardly obtained from well-known circuit analysis methods.

A. Energy as a Fundamental Link

We now focus on energy transfer across subsystems. First, note that the consistency of Kirchhoff's relations in the torque control loops allow us to merge the control and stator subsystems in Figs. 3 and 2, respectively, without any additional steps (see [3]). Shifting focus to the electrical-mechanical link, it is necessary to lay some groundwork.

Power absorbed by $\mathcal{E}_\mathrm{d}$ and $\mathcal{E}_\mathrm{q}$ is converted into electrically-induced mechanical power as described in (10). Further analysis reveals the following electrical-mechanical relations:

$$\mathcal{E}_\mathrm{q} = \left(\lambda\frac{p}{2}\right)\omega_\mathrm{m}, \quad i_\mathrm{q} = \left(\lambda\frac{p}{2}\right)^{-1}\tau_\mathrm{q} \tag{13}$$

$$\mathcal{E}_\mathrm{d} = \frac{p}{2}(L_\mathrm{d} - L_\mathrm{q})i_\mathrm{q}\omega_\mathrm{m}, \;\; i_\mathrm{d} = \left(\frac{p}{2}(L_\mathrm{d} - L_\mathrm{q})i_\mathrm{q}\right)^{-1}\tau_\mathrm{d} \tag{14}$$

Inspection of (13) and (14) show that torque contributions map to currents on their respective axes and back EMF voltages depends on mechanical speed. Most importantly, we observe that $\lambda p/2$ and $(p/2)(L_\mathrm{d} - L_\mathrm{q})i_\mathrm{q}$ act like ideal transformer turns ratios. This insight allows us to merge the stator and mechanical circuits in Figs. 2 and 4 together via a pair of ideal transformers. Ultimately, we obtain the unified circuit with control, electrical, and mechanical domains in Figure 5.

B. Linking Controls and Circuit Analysis

Next, we evaluate the closed-loop behavior of the torque and speed control loops in Fig. 5 via circuit analysis . Our aim is to

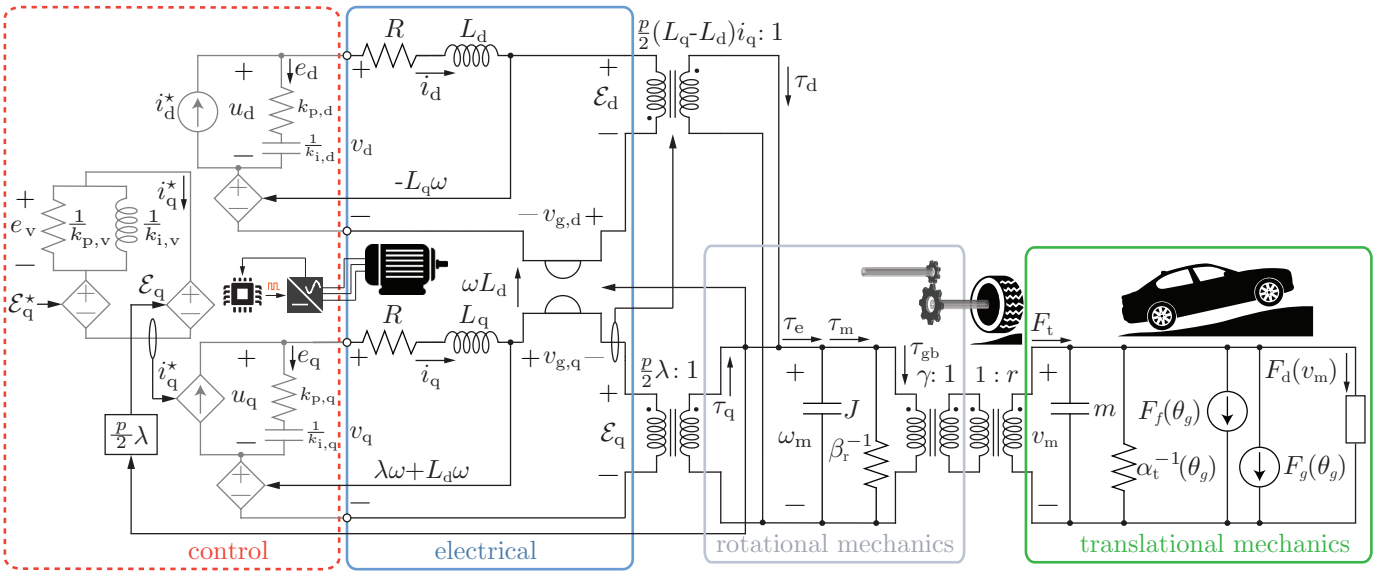

Fig. 5: A unified equivalent circuit model for a drive system with controls.

show that classical results, which are typically derived through the lens of control theory, can be reproduced with greater ease via circuit tricks. First, consider the current controller RC circuit equivalents, $z_{\mathrm{c,d}}(s)$ and $z_{\mathrm{c,q}}(s)$, which regulate torque. Denote the impedance of the stator d and q axis branches as $z_{\mathrm{s,d}}(s) := sL_{\mathrm{d}} + R$ and $z_{\mathrm{s,q}}(s) := sL_{\mathrm{q}} + R$, respectively. Assuming ideal feedforward, disturbances introduced by the gyrator cross-coupling and back EMFs are fully rejected. This follows after evaluating Kirchhoff's Voltage Law around the d and q axis circuits and disturbance voltage cancellation. The current divider equation directly gives us

$$i_{\mathrm{q}}(s) = \frac{z_{\mathrm{c,q}}(s)}{z_{\mathrm{s,q}}(s) + z_{\mathrm{c,q}}(s)} i_{\mathrm{q}}^{\star}(s) \tag{15}$$

$$= \frac{T_{\mathrm{i,q}}(s)}{1 + T_{\mathrm{i,q}}(s)} i_{\mathrm{q}}^{\star}(s) \tag{16}$$

$$i_{\mathrm{d}}(s) = \frac{z_{\mathrm{c,d}}(s)}{z_{\mathrm{s,d}}(s) + z_{\mathrm{c,d}}(s)} i_{\mathrm{d}}^{\star}(s) \tag{17}$$

$$= \frac{T_{\mathrm{i,d}}(s)}{1 + T_{\mathrm{i,d}}(s)} i_{\mathrm{d}}^{\star}(s). \tag{18}$$

The well-known relations in (16) and (18), which are known as a *complementary sensitivity function* in the controls literature, follow after defining the loop gains as $T_{\mathrm{i,q}}(s) := z_{\mathrm{c,q}}(s)/z_{\mathrm{s,q}}(s)$ and $T_{\mathrm{i,d}}(s) := z_{\mathrm{c,d}}(s)/z_{\mathrm{s,d}}(s)$ and some algebraic manipulations. This establishes a link between fundamental relations in the controls and circuits domains.

Next, the mechanical system impedance projected across the electromechanical transformer equivalent towards the stator is

$$z_{\mathrm{m}}(s) := \left(\beta_{\mathrm{net}}^{-1}(\theta_{\mathrm{g}}) \left\| \frac{1}{sJ_{\mathrm{net}}} \right.\right) \left(\frac{\lambda p}{2}\right)^2, \tag{19}$$

where $J_{\mathrm{net}} := J + m(r/\gamma)^2$ mimics a net capacitance and

$$\beta_{\mathrm{net}}(\theta_{\mathrm{g}}) := \beta_{\mathrm{r}} + \left(\alpha_t(\theta_{\mathrm{g}}) + \left.\frac{dF_{\mathrm{d}}(v_{\mathrm{m}})}{dv_{\mathrm{m}}}\right|_{v_{\mathrm{m}}=V_{\mathrm{m}}}\right) \left(\frac{\gamma}{r}\right)^2 \tag{20}$$

is the net mechanical conductance of the linearized system at grade θ_{g} and quiescent velocity V_{m}. Hence, $z_{\mathrm{m}}(s)$ is the impedance of the linearized mechanical system observed from the stator perspective. The speed control circuit carries current $i_{\mathrm{q}}^{\star}$ as given by

$$i_{\mathrm{q}}^{\star}(s) = \frac{\mathcal{E}_{\mathrm{q}}^{\star}(s) - \mathcal{E}_{\mathrm{q}}(s)}{z_{\mathrm{c,v}}(s)} \tag{21}$$

where we recall $z_{\mathrm{c,v}}(s) := k_{\mathrm{p,v}}^{-1} \| s k_{\mathrm{i,v}}^{-1}$ captures the impedance of the RL equivalent speed compensator. The voltage drop across $z_{\mathrm{m}}(s)$ equals the back EMF such that

$$\mathcal{E}_{\mathrm{q}}(s) = i_{\mathrm{q}}(s) z_{\mathrm{m}}(s), \tag{22}$$

$$= \frac{z_{\mathrm{c,q}}(s)}{z_{\mathrm{s,q}}(s) + z_{\mathrm{c,q}}(s)} i_{\mathrm{q}}^{\star}(s) z_{\mathrm{m}}(s), \tag{23}$$

$$= \frac{z_{\mathrm{c,q}}(s)}{z_{\mathrm{s,q}}(s) + z_{\mathrm{c,q}}(s)} \frac{\mathcal{E}_{\mathrm{q}}^{\star}(s) - \mathcal{E}_{\mathrm{q}}(s)}{z_{\mathrm{c,v}}(s)} z_{\mathrm{m}}(s). \tag{24}$$

where the second line utilizes (15) and the final expression results after substituting (21) for $i_{\mathrm{q}}^{\star}(s)$. Solving for $\mathcal{E}_{\mathrm{q}}(s)$ gives the closed-loop relation

$$\mathcal{E}_{\mathrm{q}}(s) = \frac{z_{\mathrm{c,q}}(s) z_{\mathrm{m}}(s)}{(z_{\mathrm{s,q}}(s) + z_{\mathrm{c,q}}(s)) z_{\mathrm{c,v}}(s) + z_{\mathrm{c,q}}(s) z_{\mathrm{m}}(s)} \mathcal{E}_{\mathrm{q}}^{\star}(s) \tag{25}$$

$$= \frac{T_{\mathrm{v}}(s)}{1 + T_{\mathrm{v}}(s)} \mathcal{E}_{\mathrm{q}}^{\star}(s) \tag{26}$$

where the loop gain, $T_{\mathrm{v}}(s) := z_{\mathrm{c,q}}(s) z_{\mathrm{m}}(s) / ((z_{\mathrm{s,q}}(s) + z_{\mathrm{c,q}}(s)) z_{\mathrm{c,v}}(s))$, in (26) is a ratio of impedances. Note that the closed-loop relation in (25) resembles a voltage divider expression and was derived entirely through basic circuit manipulations. The result in (25) may be expressed in terms of mechanical speeds (i.e., ω_{m} and $\omega_{\mathrm{m}}^{\star}$) by simply multiplying both sides by $2/(\lambda p)$.

V. Simulation Results

Here, we carry out a side-by-side comparison of, i) a conventional switch-level simulation that mirrors the structure

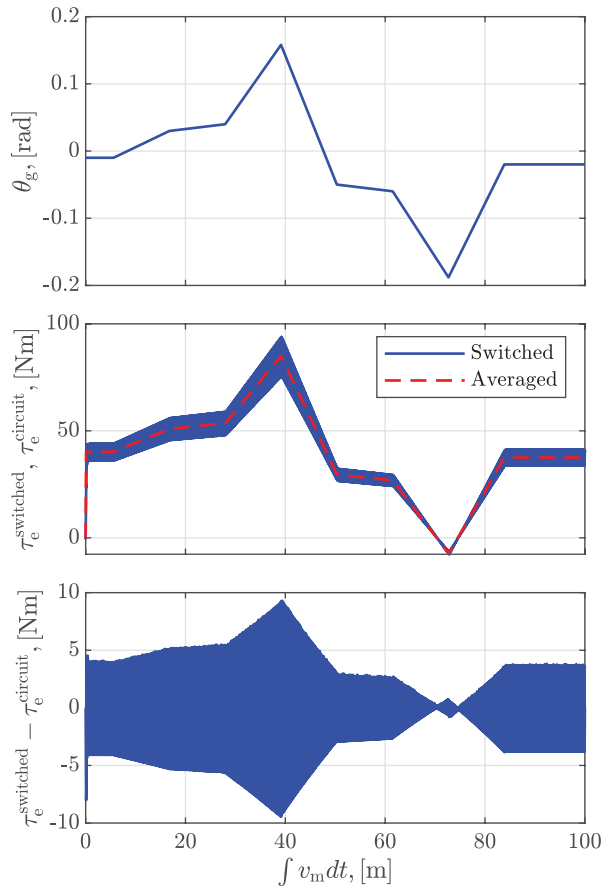

Fig. 6: (Top) Position versus grade data used in time-domain simulations. (Middle) Closed-loop torque profile for both switched and averaged equivalent circuit simulations. (Bottom) Difference between conventional switched and circuit-based simulations.

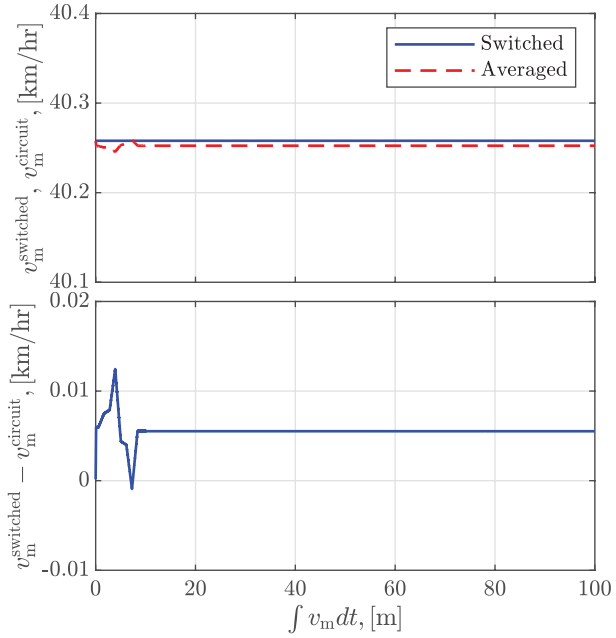

Fig. 7: (Top) Velocity under a fixed speed reference shown for the conventional switched and equivalent circuit simulations. (Bottom) Velocity difference between the two simulations.

Table I: Simulation Parameters for Case Studies.

$v_m^\star$=40.25km/hr	L_d= 24.3μH	L_q= 26.3μH
R=5mΩ	$\lambda = 33\text{mV s/rad}$	$p = 20$
$\beta_r = 80 \times 10^{-3} \frac{\text{Nm s}}{\text{rad}}$	$J = 103.5\text{kg m}^2$	$m = 1000\text{kg}$
$\gamma = 10$	$r = 320\text{mm}$	$A_f = 2.20\text{m}^2$
$C_d = 280 \times 10^{-3}$	$f_v = 16 \times 10^{-3}\text{s/m}$	$f_0 = 16 \times 10^{-3}$
$k_{p,d} = k_{p,q} = 3.14\Omega$	$k_{i,d} = 15.3 \times 10^{-3} \frac{1}{\text{F}}$	$\rho = 1.23\text{kg/m}^3$
$k_{i,q} = 16.5 \times 10^{-3} \frac{1}{\text{F}}$	$k_{p,v} = 59.9 \times 10^3 \Omega^{-1}$	$k_{i,v} = 46.2\text{H}^{-1}$

in Fig. 1(a), and ii) an equivalent circuit simulation assembled purely with basic circuit components along the lines of Fig. 5. Both simulations were carried out in PLECS software. The conventional simulation utilizes a standard control system block diagram, a synchronous machine block, and specialized blocks that capture mechanical behavior. In contrast, the equivalent circuit is assembled exclusively with RLC elements, transformers, a gyrator, as well as current and voltage sources. These two models are in Figure 8. We note that the gyrator and state-dependent transformer blocks in Fig. 8(b) have a mask and the internal structure contains coupled voltage and current sources. In both simulations, we modeled an EV with the parameters in Table I. The EV utilized a speed controller and was subjected to a terrain whose grade varied with position. Torque and speed waveforms for the conventional switch-level simulations are compared in Figs. 6–7, respectively. As illustrated, it is evident that the equivalent circuit captures all dynamics of the conventional simulation with the exception of ripple. It is also clear that the circuit representation elucidates system operation and bypasses the use of specialized machine and mechanical blocks which obscure low-level physics.

VI. Conclusions

In this paper, we established a multiphysics circuit equivalent that captures electrical, control, and mechanical dynamics in a unified setting. Our formulation hinges on the universality of energy across all known physics and careful application of circuit laws. The resulting circuit model allows for straightforward analysis of closed-loop dynamics using circuit tricks that are second nature to electrical engineers. The properties of the unified circuit equivalent not only give deeper insight into system operation, but also streamline closed-loop analysis. The utility of this model was demonstrated through an electric vehicle simulation where end-to-end (i.e., control-to-pavement) dynamics were captured in a circuit simulator.

Acknowledgment

We'd like to express gratitude to Bryan Lieblick at Plexim GmbH for providing gyrator and ideal transformer blocks. This material is based upon work supported by the U.S. Department of Energy's Office of Energy Efficiency and Renewable Energy (EERE) under Solar Energy Technologies Office (SETO) Agreement Number EE0009025. Funding was also provided by NAVFAC Order Number N0002418F8702. Brian Johnson was supported by the Washington Research Foundation.

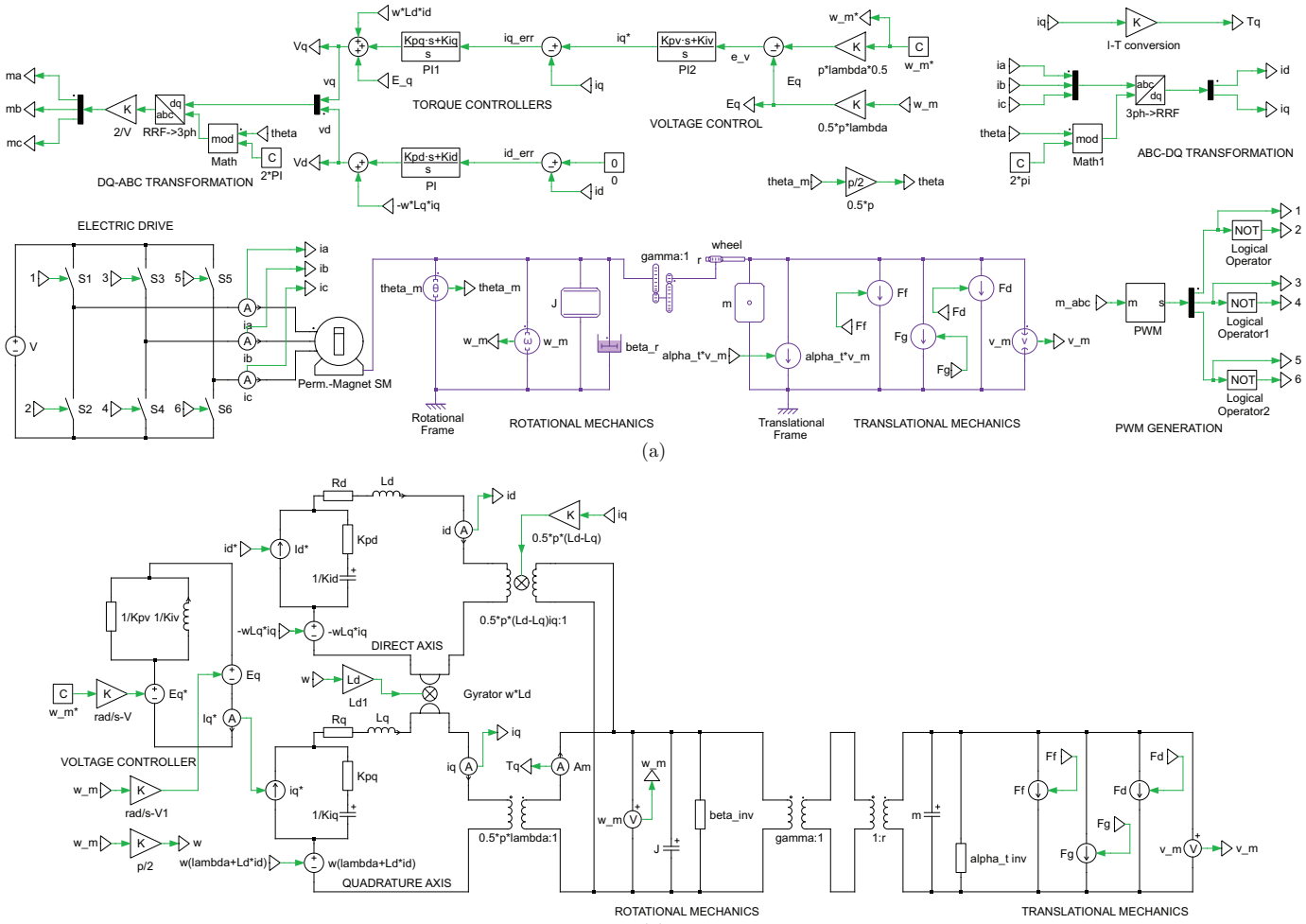

Fig. 8: The diagram in (a) shows a conventionally assembled switch-level PLECS simulation using machine and mechanics blocks which obscure internal details. Our circuit equivalent model in (b) reveals the multiphysics operation in a lucid manner using standard circuit elements.

REFERENCES

[1] R. Erickson and D. Maksimovic, *Fundamentals of Power Electronics*. Power electronics, Springer US, 2001.

[2] R. Bishop, *Mechatronics: An Introduction*. CRC Press, 2017.

[3] B. Johnson, M. Lu, V. Purba, and S. Dhople, "A circuit-equivalent model for current-controlled grid-tied inverters," in *Workshop on Control and Modeling of Power Electronics*, pp. 1–7, June 2019.

[4] R. Mallik, B. Majmunovic, S. Mukherjee, S. Dutta, G. Seo, D. Maksimovic, and B. Johnson, "Equivalent circuit models of voltage-controlled dual active bridge converters," in *Workshop on Control and Modeling of Power Electronics*, pp. 1–4, Jun. 2019.

[5] R. D. Middlebrook, "A continuous model for the tapped-inductor boost converter," in *IEEE Power Electronics Specialists Conference*, pp. 63–79, June 1975.

[6] S. R. Sanders and G. C. Verghese, "Synthesis of averaged circuit models for switched power converters," *IEEE Transactions on Circuits and Systems*, vol. 38, pp. 905–915, Aug. 1991.

[7] J. Sun, "Small-signal methods for AC distributed power systems - A review," *IEEE Transactions on Power Electronics*, vol. 24, pp. 2545–2554, Nov. 2009.

[8] X. Wang, L. Harnefors, and F. Blaabjerg, "Unified impedance model of grid-connected voltage-source converters," *IEEE Transactions on Power Electronics*, vol. 33, pp. 1775–1787, Feb. 2018.

[9] S. Chapman, *Electric Machinery Fundamentals*. McGraw-Hill, 2005.

[10] P. Kundur, N. Balu, and M. Lauby, *Power System Stability and Control*. EPRI power system engineering series, McGraw-Hill Education, 1994.

[11] K. Lambert, "The uses of analogy: James Clerk Maxwell's 'On Faraday's lines of force' and early Victorian analogical argument," *The British Journal for the History of Science*, vol. 44, no. 1, pp. 61–88, 2011.

[12] C. de Silva, *Vibration: Fundamentals and Practice*. Taylor & Francis, 2006.

[13] H. Tilmans, "Equivalent circuit representation of electromechanical transducers: I. Lumped parameter systems," *Journal of micromechanics and microengineering*, vol. 6, no. 1, 1996.

[14] W. Lin, C. Tsai, and C. Lin, "Analysing the linear equivalent circuits of electromechanical systems for steam turbine generator units," *IET Generation, Transmission Distribution*, vol. 5, no. 7, 2011.

[15] A. Yildiz, "Electrical equivalent circuit based modeling and analysis of direct current motors," *International journal of electrical power energy systems*, vol. 43, no. 1, 2012.

[16] J. Routex, S. Gay-Desharnais, and M. Ehsani, "Modeling of hybrid electric vehicles using gyrator theory: application to design," in *Proceedings of IEEE VTS Fall Vehicular Technology Conference 2000*, vol. 5, pp. 2090–2094, 2000.

[17] J. Routex, S. Gay-Desharnais, and M. Ehsani, "Study of hybrid electric vehicle drive train dynamics using gyrator-based equivalent circuit modeling," in *SAE 2002 World Congress Exhibition*, 2002.

[18] M. Ehsani, Y. Gao, S. Longo, and K. Ebrahimi, *Modern Electric, Hybrid Electric, and Fuel Cell Vehicles*. CRC Press, 2018.

[19] B. D. H. Tellegen, "The gyrator, a new electric network element," *Philips Res. Rep.*, vol. 3, pp. 81–101, Apr. 1948.